# DETECTION AND PERFORMANCE ANALYSIS FOR A MOVING POINT SOURCE IN SPECKLE NOISE, APPLICATION TO EXOPLANET DETECTION BY DIRECT IMAGING.

*I. Smith, A. Ferrari and M. Carbillet*

LUAN, Université de Nice-Sophia-Antipolis, 06108 Nice cedex 2, France

Isabelle.SMITH@unice.fr, ferrari@unice.fr, Marcel.CARBILLET@unice.fr

## ABSTRACT

With the current development of astronomical instruments able to detect the direct light of exoplanets, such as the Very Large Telescope instrument SPHERE, statistical tools need to be developed in order to make precise detection and estimation assessments. We propose a detection algorithm that delivers an estimation of the position and the intensity of the potentially detected exoplanet. Because of the numerical constraints on the signal processing task, the detector-estimator is based on a simplified Gaussian model where we use a field-rotation effect as the main discriminating criterium between the planet and the speckles. However, for a given threshold on the statistics test, the Probability of False Alarm (PFA) and the Probability of Detection (PD) need to be accurate. For that purpose we use a more realistic model and the saddlepoint approximation to compute the PFA and PD. The performance of the approximation is evaluated on a 1D data model.

***Index Terms—*** Signal detection, Object detection, Speckle, Estimation, Astronomy

## 1. INTRODUCTION AND SUMMARY

The Very Large Telescope Planet Finder SPHERE (Spectro-Polarimetric High Contrast Exoplanet REsearch), that will include extreme adaptative optics (AO) and high-contrast coronagraphy, is under development [1]. To detect exoplanets from a set of images, the main difficulty comes from the combination of residual speckles uncorrected by the adaptive optics and static aberrations of the optical system. The diffraction pattern of the static aberration of the instrument being similar to the unresolved exoplanet profile, detection algorithm proposed in the literature tries to discriminate the planet from the background by the detection of its motion. Previous work tries to suppress and stabilize the background using differential processing of successive images [2, 3].

The present paper adopts a statistical modeling approach and proposes to estimate the intensity and position of the unknown source. The true data model distribution being intractable, this is achieved using a simple test based on a Gaussian data model which leads to a practical detector for the large amount of astrophysical data (typically 1200 images of $150 \times 150$ pixels for a 3 hour run). Then a crucial point for the exoplanet detection problem is to precisely relate the detection threshold to the probability of false alarm (PFA) and the probability of detection (PD). This requires evaluating the detection performances of the test using the true data model. The marginal distribution of each pixel intensity has been shown to be Rician, except for pixels located at the center of the image [4]. Therefore the true data model cannot be reduced to a Gaussian distribution. It is also important to note that the simulation of realistic data sets using for example the software package *CAOS* [5] or the software package SPHERE [6] is extremely time demanding and does not allow to obtain PD and PFA using Monte Carlo simulations. Unlike the direct distribution, the moment generating function (MGF) of the speckle model is reachable. Consequently we propose to use the saddlepoint approximation in order to derive the PFA-threshold relation and evaluate the quality of the estimator through the Receiver Operating Characteristic (ROC) curve.

This paper is organized as follows. Section 2 presents the statistical properties of the observed data. Section 3 is devoted to the detection algorithm using the simplified model. Section 4 evaluates the performance of the test using the exact data model. Conclusions are reported in section 5.

## 2. DATA MODEL

### 2.1. Distribution of the intensities

The dataset consists in $N$ successive images. The intensity on image $k$ is represented by a $M \times 1$ vector $\boldsymbol{i}_k$ which results from the contribution of the star light $\boldsymbol{u}_k$ and the planet light. The vector $\boldsymbol{u}_k$ is associated to a $M \times 1$ vector containing the intensities $u_k(\ell) = |\psi_k(\ell)|^2$ in the focal plane of the telescope which arise from the propagation of the star light wavefront through the atmosphere, the adaptive optic and the coronagraph which will reduce the diffraction of the star light. A straightforward extension of the high flux model derived in [7] to the multivariate case leads to a decomposition of the complex amplitude $\boldsymbol{\psi}_k$ in two terms $\boldsymbol{\psi}_k = \boldsymbol{\mu} + \boldsymbol{\phi}_k$

- The first, $\boldsymbol{\mu} \in \mathbb{C}^M$, models the static impulse response of the coronagraph and the static aberrations (e.g. lens defaults) of the optical system. This deterministic term plays a central role in the planet detection problem [4].
- The second term models the residuals of atmospheric turbulence that are not corrected by the adaptive optics system and that propagate through the coronagraph. This term is assumed to be a complex zero-mean circular Gaussian vector, i.e. $\mathsf{E}[\boldsymbol{\phi}_k \boldsymbol{\phi}_k^H] = \Sigma$ and $\mathsf{E}[\boldsymbol{\phi}_k \boldsymbol{\phi}_k^t] = 0$, see [8].

The presence of a planet at the *unknown position* $r$ results in a similar model for the complex amplitude where the deterministic part is the response of the system to a point source located in $r$ (note that due to the coronagraph this response is not shift invariant). However, for an extreme adaptive optics, the atmospheric turbulence residuals can be neglected with respect to the central part of this response. Consequently the presence of a planet on the first image at the *unknown position* $r$ results in the deterministic response $\alpha \boldsymbol{p}_k(r)$ where $\alpha$ is the *unknown intensity* of a possible planet, and $\boldsymbol{p}_k(r)$ is the *known instrumental response* of the source at time $k$. Note that this model assumes that not only the instantaneous profile is known

1-4244-1484-9/08/$25.00 ©2008 IEEE

but also the trajectory of the source, which is the case for a telescope with an alt-azimuthal mount.

Consequently we will consider that:

$$\boldsymbol{i}_k = \boldsymbol{u}_k + \alpha \boldsymbol{p}_k(r), \text{ with } u_k(\ell) = |\psi_k(\ell)|^2 \tag{1}$$

where $\boldsymbol{\psi}_k \sim \mathcal{N}_c(\boldsymbol{\mu}, \Sigma)$. Moreover the successive vectors $\boldsymbol{\psi}_k$, $k = 1 \dots N$ are assumed to be independent.

Gaussian circularity for a 1-dimensional random variable implies that its real and imaginary part are independent with identical variance. Consequently Eq. (1) shows that $u_k(\ell)$ is proportional to a random variable distributed according to a noncentral $\chi^2$ distribution with 2 degrees of freedom [9]. The multivariate distribution of $\boldsymbol{u}_k$ is much more complicated to derive. It can be obtained by noting that $\boldsymbol{u}_k$ is the diagonal of the $M \times M$ matrix $\boldsymbol{\psi}_k \boldsymbol{\psi}_k^H$ which has a noncentral complex Wishart distribution [10]. Consequently, the distribution of $\boldsymbol{u}_k$ is the ad-hoc marginal of this distribution. Unfortunately analytical computation of its probability distribution function is intractable in the general case.

The expression of the moment generating function of a noncentral complex Wishart distribution gives immediately the following closed form expression for the $\boldsymbol{u}_k$ MGF:

$$h_{\boldsymbol{u}_k}(\boldsymbol{s}) = \mathsf{E}[e^{-\boldsymbol{u}_k^t \boldsymbol{s}}] = \frac{e^{-\boldsymbol{\mu}^H D_{\boldsymbol{s}}(I+\Sigma D_{\boldsymbol{s}})^{-1}\boldsymbol{\mu}}}{|I + \Sigma D_{\boldsymbol{s}}|} \tag{2}$$

where $D_{\boldsymbol{s}}$ is the diagonal matrix $D_{\boldsymbol{s}} = \mathsf{Diag}(\boldsymbol{s})$. According to (1) the MGF of $\boldsymbol{i}_k$ is:

$$h_{\boldsymbol{i}_k}(\boldsymbol{s}) = e^{-\alpha \boldsymbol{p}_k(r)^t \boldsymbol{s}} h_{\boldsymbol{u}_k}(\boldsymbol{s}) \tag{3}$$

### 2.2. Distribution of the photocounted data

The vector of intensities $\boldsymbol{i}_k$ described above corresponds to the case where the images have been recorded under a high flux assumption. However, for low-flux objects or short exposure time, the photocounting effect has to be considered. Denote as $\boldsymbol{x}_k$ the vector of photocounts associated to the intensity $\boldsymbol{i}_k$. Conditioned upon the vector of intensities, the random variables $x_k(\ell)$, $\ell = 1, \dots, M$ are independent and distributed according to Poisson distributions with means $i_k(\ell)$, $\ell = 1, \dots, M$. Tractable expressions of $\Pr(\boldsymbol{x}_k = \boldsymbol{q})$ are obviously difficult to obtain. However, many interesting properties regarding the distribution of $\boldsymbol{x}_k$ can be derived in the multivariate case [11]. We will focus hereafter on the MGF of $\boldsymbol{x}_k$ which is related to the MGF of $\boldsymbol{i}_k$ by:

$$h_{\boldsymbol{x}_k}(\boldsymbol{z}) = \mathsf{E}[\prod_{\ell=1}^{M} z(\ell)^{x_k(\ell)}] = h_{\boldsymbol{i}_k}(\boldsymbol{1} - \boldsymbol{z}) \tag{4}$$

Figure 1 illustrates a typical simulation of the IRDIS (InfraRed Dual-beam Imaging and Spectroscopy) facility of SPHERE, obtained using the software package SPHERE v2.1[6] developed within the CAOS problem-solving environment [12] and assuming the standard simulation parameters.

## 3. DETECTION ALGORITHM

According to the model developed in the previous section, the planet detection problem consists in the composite hypothesis test:

$$H_0 : \alpha = 0, \; H_1 : \alpha > 0 \tag{5}$$

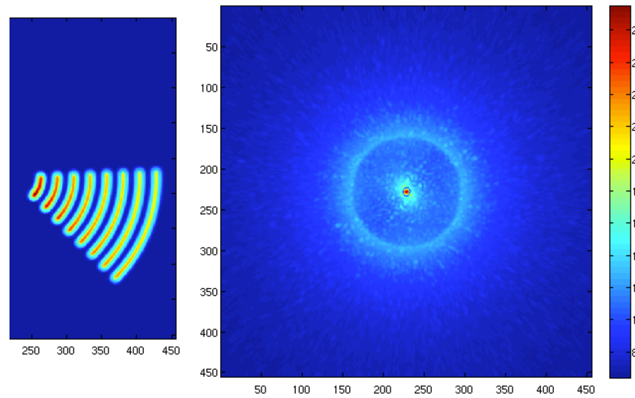


**Fig. 1**. The left image represents in a log-scale the time integration of 8 sources: $\sum_{k=1}^{N} \boldsymbol{p}_k(r)$, for 8 different initial positions $r$. The right image is the time integration of $N = 450$ simulated images: $\sum_{k=1}^{N} \boldsymbol{x}_k$, represented at the power of 0.2 again.

The distribution of $\boldsymbol{x}_k$ being intractable the derivation of a test statistics will rely on the simplified data model:

$$\boldsymbol{x}_k = \boldsymbol{d} + \alpha \boldsymbol{p}_k(r) + \boldsymbol{\epsilon}_k \tag{6}$$

where $\boldsymbol{\epsilon}_k \sim \mathcal{N}(\boldsymbol{0}, \sigma^2 I)$ and $\boldsymbol{d}$ denotes the stationary deterministic unknown instrumental response (in our case: coronagraph, static speckles, ...), and $r$ is still the unknown initial position of the exoplanet. This model can be justified under high flux assumptions. In fact it has been proved in [13] that under unrestrictive assumptions, when $\forall \ell$, $\mathsf{E}[\boldsymbol{u}_k(\ell)] \to +\infty$, a properly standardized $\boldsymbol{x}_k$ satisfying (4) will converge in distribution to a Gaussian independent distributed vector.

Maximizing the likelihood function $L(\alpha, r, \boldsymbol{d}, \sigma^2)$ under the simplified model with respect to the unknown parameters $(\alpha, \boldsymbol{d}, \sigma^2)$ for a given $r$ leads to:

$$\hat{\alpha}(r) = \sum_k \boldsymbol{w}_k(r)^t \boldsymbol{x}_k, \; \boldsymbol{w}_k(r) = \frac{N\boldsymbol{p}_k(r) - \sum_k \boldsymbol{p}_k(r)}{c_N(r)} \tag{7}$$

$$c_N(r) = N \sum_k \|\boldsymbol{p}_k(r)\|^2 - \| \sum_k \boldsymbol{p}_k(r)\|^2 \tag{8}$$

It is worthy to note that the identifiability condition for the parameters is $c_N(r) \neq 0$ which is the case as soon as at least two sources are disjointed.

The MLE estimation of $r$ is then achieved by maximizing the compressed likelihood $r \to L(\hat{\alpha}(r), r, \hat{\boldsymbol{d}}(r), .)$:

$$\hat{r}_{ML} = \arg \max_{r=1,\dots,M} \left\{ c_N(r) \hat{\alpha}(r)^2 \right\} \tag{9}$$

and from it we get $\hat{\alpha}_{ML} = \hat{\alpha}(\hat{r}_{ML})$. Note that if we can neglect the variation of the term $c_N(r)$ with respect to $r$, as this term is also positive, and if $\hat{\alpha}_{ML} > 0$, we can approximate

$$\hat{r}_{ML} \approx \arg \max_r (\hat{\alpha}(r)) \tag{10}$$

If $r$ was known, the model (6) being Gaussian and linear with respect to $(\boldsymbol{d}, \alpha)$ the MLE would be an unbiased and efficient estimator with: $\mathsf{var}(\hat{\alpha}_{ML}) = N\sigma^2 c_N(r)^{-1}$ But actually, since $r$ is unknown, the model is not linear in the parameters. Furthermore,

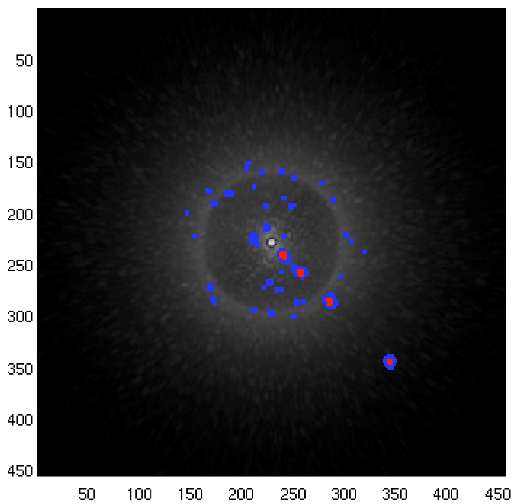


**Fig. 2**. Thresholded map (2 levels) of $\hat{\alpha}(r)$ obtained from the data of figure 1 and superimposed on $\sum \boldsymbol{x}_k$. The 4 simulated exoplanets located at $0\overset{''}{.}2$, $0\overset{''}{.}5$, $1''$ and $2''$ and 1.6 $10^{-6}$ times less bright than the central star are correctly detected with the first threshold.

due to the motion of the source $\boldsymbol{p}_k$, the model $\boldsymbol{x}_k = \boldsymbol{s}_k(\boldsymbol{\theta}) + \boldsymbol{\epsilon}_k$, $\boldsymbol{\epsilon}_k \sim \mathcal{N}(0, \sigma^2 I)$ does not correspond to a standard one where the $\boldsymbol{x}_k$ would be i.i.d. However, generalizing the proof of the proposition IV.E.1 from [14] to the case of a non-scalar parameter $\boldsymbol{\theta}$, it can be can proved that $\hat{\boldsymbol{\theta}}_{ML}$ is asymptotically consistent anyway.

According to these results we propose the test:

$$H_0 \text{ rejected if } \hat{\alpha}_{ML} > \zeta \tag{11}$$

where the threshold $\zeta$ depends on the required probability of false alarm (PFA). Note that since the data do not actually satisfy the model used in the MLE, we do not use the Generalize Likelihood Ratio Test and keep $\hat{\alpha}$ as the simple test statistics used. Figure 2 shows a thresholded map of $\hat{\alpha}(r)$.

## 4. DETECTION LEVEL

### 4.1. Saddlepoint approximation

The purpose of this section is the evaluation of the performances of the detection scheme (11) when applied to the data distributed according to the model described in section 2. This is achieved assuming that $r$ is known. In order to simplify the notation, the dependence on $r$ will be dropped in the sequel.

Taking benefit of the existence of an analytic expression of the MGF and from our interest in the tails of the distribution for the computation of PFA and PD, we use the standard saddlepoint approximation [15]. Assuming that we are concerned by cases where $\mathsf{E}[\hat{\alpha}] < \zeta$ under $H_0$ and $\mathsf{E}[\hat{\alpha}] > \zeta$ under $H_1$, we use the following expressions of the saddlepoint approximation: if $h_i(z)$ denotes the MGF of the test statistic under $H_i$,

$$P_{FA}(\zeta) \approx -(2\pi\phi_0''(z_0))^{-1/2} e^{\phi_0(z_0)} \tag{12}$$

$$P_D(\zeta) \approx 1 - (2\pi\phi_1''(z_1))^{-1/2} e^{\phi_1(z_1)} \tag{13}$$

$$\phi_i(z) = \frac{h_i(z)e^{\zeta z}}{n(i)z}, \quad n(0) = -1, \quad n(1) = 1 \tag{14}$$

where the saddlepoints $z_0 < 0$ and $z_1 > 0$ satisfy

$$\phi_i'(z_i) = 0, \quad z_0 < 0, \quad z_1 > 0. \tag{15}$$

However, although for continuous and integers random variables these saddlepoint approximations are well known, in our case $\hat{\alpha}$ is a linear combination of integers (see Eq. (7)) so $\hat{\alpha}$ ranges in a discrete but not integer set. This raises a difficulty for the definition of the MGF. A similar problem occurs in [16] where the authors approximate the discrete random variables by continuous random variables. Approximating $\hat{\alpha}$ by a continuous random variable is justified in [17] by showing that the relative error of the approximation decreases as rapidly as $N$ increases. Then we use the expressions above and

$$h_1(z) = \mathsf{E}[e^{-z\hat{\alpha}}] = \prod_{k=1}^{N} \mathsf{E}[e^{-z\boldsymbol{w}_k^t \boldsymbol{x}_k}] = \prod_{k=1}^{N} h_{\boldsymbol{x}_k}(e^{-z\boldsymbol{w}_k}) \tag{16}$$

where $e^{\boldsymbol{u}} \triangleq (e^{u(1)}, \ldots, e^{u(M)})^t$. Substituting Eqs. (4,3,2) in (16) gives:

$$\ln(h_1(z)) = -\alpha \sum_k (\mathbf{1} - e^{-z\boldsymbol{w}_k})^t \boldsymbol{p}_k + \ln(h_0(z)) \tag{17}$$

with:

$$\ln(h_0(z)) = -\sum_k \ln|I + \Sigma(I - D_{e^{-z\boldsymbol{w}_k}})| - \boldsymbol{\mu}^H \sum_k (I - D_{e^{-z\boldsymbol{w}_k}})(I + \Sigma(I - D_{e^{-z\boldsymbol{w}_k}}))^{-1}\boldsymbol{\mu} \tag{18}$$

Computation of the first and second order derivatives of $\phi_0(z)$ is obtained from (18) using $(\ln|A(z)|)' = -\mathrm{Tr}(A(z)^{-1}A(z)')$ and $(A(z)^{-1})' = -A(z)^{-1}A(z)'A(z)^{-1}$.

Note that the computation of the saddlepoint approximation does not necessarily involve the resolution of the equation $\phi_0'(z_0) = 0$, especially if we want to describe a large set of thresholds. In practice we let $z_0$ vary on the negative real axis and $z_1$ on the positive real axis, and compute simply the corresponding threshold from a reexpression of (14,15):

$$\zeta = \frac{1}{z_i} - \frac{d\ln(h_i(z))}{dz}|_{z=z_i} \tag{19}$$

### 4.2. Simulation results

The saddlepoint approximation used to derive the PFA and PD for (17) and (18) has been validated using a simple 1D model where $M = 30$ and $N = 10$; the $\boldsymbol{\psi}_k$ are generated according to a first order circular Gaussian autoregressive process with covariance matrix $\Sigma_{i,j} = c_0\rho^{|i-j|}e^{\jmath\varphi(j-i)}$ and with parameters $\boldsymbol{\mu} = 0.08 \times \mathbf{1}$, $\phi = \pi/4$, $\rho = 0.85$ and $c_0 = 1$; the source is uniformly accelerated and its profile is chosen static with a characteristic size similar to the correlation pattern induced by $\Sigma$; the datasets are simulated under $H_0$ ($\alpha = 0$) and $H_1$ with $\alpha = 0.5$; $10^6$ independent datasets are simulated and tested for $H_0$ and $H_1$.

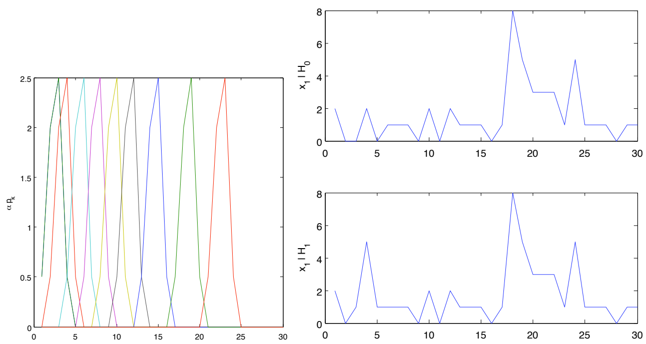

**Fig. 3**. Left: Source profiles $\alpha \boldsymbol{p}_k$ for $k = 1...10$ (note $\boldsymbol{p}_1 = \boldsymbol{p}_2$). Right: realization of $\boldsymbol{x}_1$ under $H_0$ (top) and $H_1$ (bottom).

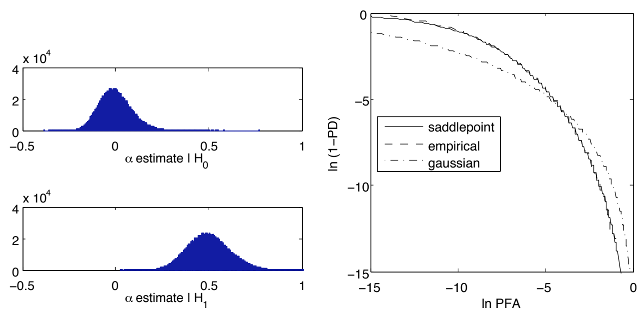


**Fig. 4**. Left: Histograms of $\hat{\alpha}$ under $H_0$ (top) and $H_1$ (bottom). Right: ROC curve where $\ln(1 - P_D)$ is a function of $\ln(P_{FA})$ (see text for the legend).

Figure 3 shows some resulting simulation plots. Figure 4 shows on the left the histograms of $\hat{\alpha}$ obtained under $H_0$ and $H_1$, and on the right it shows the ROC curve in a log view, computed in three different ways: first the PFA and PD are computed according to the saddlepoint approximation (13,14), then empirically, using respectively the $H_0$ and the $H_1$ histograms of $\hat{\alpha}$, and finally assuming that $\hat{\alpha}$ is normally distributed, with moments estimated from the same empirical distributions as in the previous ROC curve. Figure 5 shows these same probabilities but now as functions of the threshold $\zeta$ and stressing the transition domain between high PFA and low PD. It is interesting to note that the probability density function of $\hat{\alpha}$ under $H_0$ is slightly skewed, so that the saddlepoint approximation better approximates the empirical distribution than the Gaussian one. And on Fig. 5, we remark that this effect is less visible for $P_D$ than $P_{FA}$, which can be interpreted within the frame of the approximation made to justify the simplified model (6): the presence of the source increases the mean flux so that the data is better approximated by a normal distribution.

## 5. CONCLUSION AND OUTLOOK

Thanks to the test statistics derived and the accurate model used to evaluate these statistics, we saw that the saddlepoint approximation gives good and better estimates of PFA and PD than a Gaussian one. But taking a simulation case with a lower signal leads to a less accurate approximation: a threshold corresponding to PFA $\sim 10^{-3}$

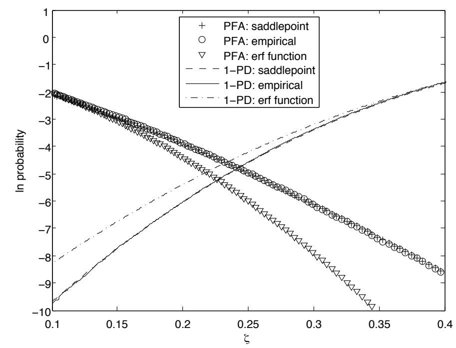


**Fig. 5**. Logarithms of $P_{FA}$ and $1 - P_D$ as function of the threshold, computed from the saddlepoint approximation.

would not correspond anymore to a low PD. Then, we should probably prefer a development in Edgeworth series for PD[15]. Moreover, we still need to find estimators of $\boldsymbol{\mu}$ and $\Sigma$ and check that we finally did have found a practical approximation to estimate PFA and PD testing it on large astronomical datasets.

## 6. REFERENCES


[1] F. Wildi et al., "The SPHERE exoplanet imager: Status report at PDR," in *SPIE*, 2007.

[2] C. Marois, D. Lafrenière, R. Doyon, B. Macintosh, and D. Nadeau, "Angular Differential Imaging: A Powerful High-Contrast Imaging Technique," *The Astrophysical Journal*, vol. 641, pp. 556–564, Apr. 2006.

[3] L.M. Mugnier, J.-F. Sauvage1, T. Fusco, and G. Rousset, "Multi-channel planet detection algorithm for angular differential imaging," in *Optical Society of America*, 2007.

[4] R. Soummer, A. Ferrari, C. Aime, and L. Jolissaint, "Speckle noise and dynamic range in coronagraphic images," *The Astrophysical Journal*, vol. 669, pp. 642–656, nov 2007.

[5] M. Carbillet, C. Vérinaud, B. Femenía, A. Riccardi, and L. Fini, "Modelling astronomical adaptive optics: I. the software package caos," *Monthly Notices of the Royal Astronomical Society*, 2004.

[6] A. Boccaletti et al., "Simulation tool manual for software package sphere v2.1," Tech. Rep., VLT-MAN-SPH-14690-0230, 2007.

[7] C. Aime and R. Soummer, "Influence of speckle and Poisson noise on exoplanet detection with a coronagraph," in *European Signal Processing Conference*, 2004.

[8] Bernard Picinbono, *Random Signals and Systems*, Pearson US Imports & PHIPEs, 1993.

[9] N. L. Johnson, S. Kotz, and N. Balakrishnan, *Continuous Univariate Distributions*, vol. 2, John Wiley, New York, 2nd edition, 1995.

[10] Robb J Muirhead, *Aspects of multivariate statistical theory*, Wiley series in probability and mathematical statistics. Wiley, New York, 1982.

[11] A. Ferrari, G. Letac, and J.-Y. Tourneret, "Multivariate mixed Poisson distributions," in *EUSIPCO*, Vienna, 2004.

[12] M. Carbillet et al., "Caos: a numerical simulation tool for astronomical adaptive optics (and beyond)," in *SPIE Proceedings*, 2004, vol. 5490, p. 637.

[13] A. Ferrari, J.Y. Tourneret, and G. Alengrin, "Parametric modeling of photometric signals," *EURASIP Signal Processing*, vol. 82, pp. 649–661, 2002.

[14] H. Vincent Poor, *An Introduction to Signal Detection and Estimation*, Springer, 1998.

[15] Carl W Helstrom, *Elements of signal detection and estimation*, PTR Prentice Hall, Englewood Cliffs, N.J., 1995.

[16] S. A. Aldosari and J.M.F Moura, "Detection in sensor networks: The saddlepoint approximation," *IEEE Transactions on Signal Processing*, vol. 55, no. 1, pp. 327–340, jan 2007.

[17] James G. Booth, Peter Hall, and Andrew T. A. Wood, "On the validity of edgeworth and saddlepoint approximations," *Journal of Multivariate Analysis Anal.*, vol. 51, no. 1, pp. 121–138, 1994.